C. R. Mecanique 346 (2018) 756–769

Contents lists available at ScienceDirect

Comptes Rendus Mecanique

www.sciencedirect.com

Computational modeling of material forming processes / Simulation numérique des procédés de mise en forme

Prediction of plastic anisotropy of textured polycrystalline sheets using a new single-crystal model

Nitin Chandola, Oana Cazacu *, Benoît Revil-Baudard

Department of Mechanical and Aerospace Engineering, University of Florida, REEF, 1350 N. Poquito Rd., Shalimar, FL 32579, USA

ARTICLE INFO

Article history:
Received 26 September 2017
Accepted 30 April 2018
Available online 15 June 2018

Keywords:
Single-crystal yield criterion
Ideal textures
Lankford coefficients
Texture effects

ABSTRACT

In this paper, we predict the effect of texture on the plastic anisotropy and consequently the drawing performance of polycrystalline metallic sheets. The constituent grain behavior is modeled using the new single-crystal yield criterion developed by [1]. For ideal texture components, the yield stress and plastic strain ratios can be obtained analytically. For the case of strongly textured sheets containing a spread about the ideal texture components, the polycrystalline response is obtained numerically on the basis of the same single-crystal criterion. It is shown that for textures obtained with rotationally symmetric misorientations of scatter width of up to 35° from the ideal orientation, the numerical predictions have the same trend as those obtained analytically for an ideal texture, but the anisotropy is less pronounced. Furthermore, irrespective of the number of grains in the sample, Lankford coefficients have finite values for all loading orientations. Illustrative examples for sheets with textures containing a combination of few ideal texture components are also presented. The simulations of the predicted polycrystalline behavior based on the new description of the plastic behavior of the constituent grains capture the influence of individual texture components on the overall degree of anisotropy. The polycrystalline simulation results are also compared to analytical estimates obtained using the closed-form formulas for the ideal components present in the texture in conjunction with a simple law of mixtures. The analytical estimates show the same trends as the simulation results. Therefore, the trends in plastic anisotropy of the macroscopic properties can be adequately estimated analytically.

1. Introduction

Description of the plastic deformation of textured polycrystalline materials using advanced analytical orthotropic yield criteria that capture with accuracy the anisotropy in mechanical response of the metal in bulk have led to significant advances in metal technology. Examples of yield criteria for textured polycrystalline materials that are defined for three-dimensional loadings include [2–7].

In the framework of crystal plasticity, the most widely used approach for determining the macroscopic plastic anisotropy and its influence on formability is based on the Schmid law for activation of slip in the constituent grains and Taylor's assumption of homogeneous deformation of all crystals [8]. There is an immense body of literature and publications on the

* Corresponding author.
E-mail address: cazacu@reef.ufl.edu (O. Cazacu).

https://doi.org/10.1016/j.crme.2018.05.004
1631-0721/

Taylor model, also called Taylor–Bishop–Hill (TBH) model, [8–10]. For a review of the TBH theory the reader is referred to the enlightening contributions of [11] and [12]. While increasingly complex homogenization schemes have been proposed (e.g., see [13]), use of such models for solving large-scale boundary value problems is still limited, mainly due to the prohibitive computational cost (e.g., see [14]).

Recently, Cazacu et al. [1] developed an analytical yield criterion for cubic single crystals. It is represented by a function which is C^2 differentiable for any three-dimensional stress states, and it accounts for the symmetries of the crystal. It involves four anisotropy coefficients and as such has added flexibility compared to the classical Schmid law or the regularized form of Schmid law [15]. Specifically, the yield criterion of [1] accounts for the differences in yield stress anisotropy between single-crystals, for example it captures the different relative ordering of the yield stresses as a function of the crystallographic direction of loading in single-crystal copper as compared to aluminum single crystal.

Plastic anisotropy has pronounced effects on the strain distribution during any forming process. For example, it is generally accepted that the anisotropy in Lankford coefficients is related to the metal drawing performance (in particular, formation of "earing"), and as such is of interest to metallurgists, engineers and designers (e.g., for aluminum single crystals see mechanical data and cup drawing test results reported by [16] and [17] respectively; for polycrystalline aluminum sheets, see for example [18–22]).

In this paper, using the new yield criterion of [1] for describing the plastic behavior of the constituent crystals, we study the effect of texture on the mechanical response of polycrystalline metallic sheets. Specifically, we predict the anisotropy in uniaxial yield stresses and Lankford coefficients (r-values) in metallic sheets containing the following texture components: $\{100\}\langle 001\rangle$ (cube), $\{110\}\langle 001\rangle$ (Goss), $\{112\}\langle 11\bar{1}\rangle$ (copper), and $\{\bar{2}1\bar{1}\}\langle 011\rangle$ that are commonly observed experimentally (e.g., see [11]). First, results are presented for sheets having one texture component specified in terms of a rotationally symmetric Gaussian distribution of misorientations with scatter width ranging from 0° (i.e. ideal texture) up to 35° around the respective ideal texture component. It is shown that for ideal textures, using the single-crystal criterion of [1] the directional dependence of the yield stress and Lankford coefficients can be calculated analytically. For the case of strongly textured sheets containing a spread about the ideal texture components, the polycrystalline response is calculated numerically using the same single-crystal criterion of [1] for the description of the behavior of the constituent grains in conjunction with Sachs hypothesis of uniform stress (see [23]) in all grains. The results of simulations of the polycrystalline behavior for textures with misorientation scatter width up to 35° about the ideal orientations show similar albeit less pronounced trends in anisotropy as the analytical ones obtained for ideal textures. Irrespective of the texture component considered in the simulations, the Lankford coefficients exist and have finite values for all loadings. Next, illustrative examples for sheets with textures containing a few ideal components are presented. These polycrystalline simulations results are compared to analytical estimates obtained using the closed-form formulas for the ideal components present in the texture in conjunction with simple law of mixtures. Also, the predictions of the anisotropy in plastic properties obtained with the new polycrystal model are compared with mechanical data reported in [24] and [25] for polycrystalline aluminum sheets. We conclude with a summary of the main findings.

2. Constitutive model

Using the generalized invariants for cubic symmetry developed in [1], one can construct yield criteria that are pressure-insensitive and satisfy the invariance requirements associated with the symmetries of each of the crystal classes of the cubic system. In this paper, we will use the single-crystal yield criterion developed for the hextetrahedral, gyroidal, and hexoctahedral cubic classes. This is motivated by the fact that most of the face centered cubic metals (e.g., copper; aluminum) belong to these crystal classes.

Generally, it can be assumed that the mechanical response in tension and compression is the same; therefore, the following even function in stresses, proposed in [1], will be further considered for the description of the plastic behavior of the constituent grains:

$$\left(J_2^C\right)^3 - c\left(J_3^C\right)^2 = k^6 \tag{1}$$

where k denotes the yield limit in simple shear in any of the {100} crystallographic planes. In the above equation c is a material constant that controls the relative importance of the generalized invariants of the stress deviator, J_2^C and J_3^C, on yielding of the crystal.

In the coordinate system Oxyz associated with the $\langle 100\rangle$ crystal axes, these generalized cubic invariants are expressed as:

$$\begin{aligned} J_2^C &= \frac{m_1}{6}\left[(\sigma_{xx}-\sigma_{yy})^2+(\sigma_{xx}-\sigma_{zz})^2+(\sigma_{zz}-\sigma_{yy})^2\right]+m_2\left(\sigma_{xy}^2+\sigma_{xz}^2+\sigma_{yz}^2\right) \\ J_3^C &= \frac{n_1}{27}(2\sigma_{xx}-\sigma_{yy}-\sigma_{zz})(2\sigma_{yy}-\sigma_{zz}-\sigma_{xx})(2\sigma_{zz}-\sigma_{xx}-\sigma_{yy})+2n_4\sigma_{xy}\sigma_{xz}\sigma_{yz} \\ &\quad -\frac{n_3}{3}\left[\sigma_{yz}^2(2\sigma_{xx}-\sigma_{yy}-\sigma_{zz})+\sigma_{xz}^2(2\sigma_{yy}-\sigma_{zz}-\sigma_{xx})+\sigma_{xy}^2(2\sigma_{zz}-\sigma_{xx}-\sigma_{yy})\right] \end{aligned} \tag{2}$$

More details about the mathematical framework and the derivation of the expressions of these generalized invariants can be found in [1].

Given that the criterion given by Eq. (1) with J_2^C and J_3^C given by Eq. (2) is a homogeneous function in stresses, the yielding response is the same if the coefficients m_1, m_2, n_1, n_3, n_4 are replaced by βm_1, βm_2, βn_1, βn_3, βn_4, with β being an arbitrary positive constant. Therefore, without loss of generality one of the parameters, for example m_1, can be set equal to unity. Accordingly, the effective stress $\bar{\sigma}$ associated with this single-crystal criterion is:

$$\bar{\sigma} = \frac{3}{(27-4cn_1^2)^{1/6}} \left\{ \begin{array}{l} [\frac{1}{2}(\sigma'^2_{xx}+\sigma'^2_{yy}+\sigma'^2_{zz})+m_2(\sigma'^2_{xy}+\sigma'^2_{xz}+\sigma'^2_{yz})]^3 \\ -c[n_1\sigma'_{xx}\sigma'_{yy}\sigma'_{zz}-n_3(\sigma'_{zz}\sigma'^2_{xy}+\sigma'_{xx}\sigma'^2_{yz}+\sigma'_{yy}\sigma'^2_{xz})+2n_4\sigma'_{xy}\sigma'_{xz}\sigma'_{yz}]^2 \end{array} \right\}^{1/6} \tag{3}$$

with $\boldsymbol{\sigma}'$ denoting the Cauchy stress deviator.

Therefore, the single-crystal yield criterion involves only five independent parameters: m_2, n_1, n_3, n_4 and c. The coefficient n_1 has a clear physical significance being directly expressible in terms of the ratio between the yield limits in uniaxial tension along $\langle 100 \rangle$ directions and the yield limit in simple shear i.e. k. The remaining coefficients m_2, n_3, n_4 and c can be determined from the tensile yield stresses along four different orientations. More details concerning the identification procedure can be found in [1].

It is worth noting that the single-crystal criterion (1) is expressed by a differentiable function of class C^2 for any stress state. Assuming an associated flow rule, the plastic strain-rate tensor, $\mathbf{d}^P$, can be easily calculated as:

$$\mathbf{d}^P = \dot{\lambda}\frac{\partial \bar{\sigma}}{\partial \boldsymbol{\sigma}} \tag{4}$$

where $\dot{\lambda}$ is the plastic multiplier, and $\bar{\sigma}$ is given by Eq. (3).

To model the polycrystal behavior, we will use the single crystal model (Eqs. (1)–(4)) for the description of the constituent grains in conjunction with Sachs hypothesis (e.g., see [23]). All the grains are prescribed the same stress tensor, $\boldsymbol{\sigma}$, expressed in the loading frame. Therefore, the equivalent stress, $\bar{\sigma}_{\text{poly}}$, of the polycrystalline material as a function of the applied stress tensor $\boldsymbol{\sigma}$, expressed in the loading frame, is:

$$\bar{\sigma}_{\text{poly}}(\boldsymbol{\sigma}) = \frac{1}{N}\sum_{i=1}^{N} \bar{\sigma}^i_{\text{grain}}\left(\mathbf{R}_i^{\mathsf{T}}\boldsymbol{\sigma}\mathbf{R}_i\right) \tag{5}$$

with N being the number of grains considered in the polycrystalline material, $\bar{\sigma}^i_{\text{grain}}$ is the effective stress associated with the single-crystal criterion (3) computed for any given grain i using Eq. (3), and $\mathbf{R}_i$ is the transformation matrix for passage from the crystal axes of the grain i to the loading frame. Note that since grains have different orientations, the equivalent stress, calculated using Eq. (3), is not identical in each grain.

Using the normality rule, the plastic strain-rate deviator $\mathbf{D}^p$ of the polycrystalline material is expressed in the loading frame as:

$$\mathbf{D}^p = \frac{\dot{\lambda}}{N}\sum_{i=1}^{n} \mathbf{R}_i \frac{\partial \bar{\sigma}^i_{\text{grain}}(\mathbf{R}_i^{\mathsf{T}}\boldsymbol{\sigma}\mathbf{R}_i)}{\partial(\mathbf{R}_i^{\mathsf{T}}\boldsymbol{\sigma}\mathbf{R}_i)}\mathbf{R}_i^{\mathsf{T}} \tag{6}$$

The new polycrystalline model (Eqs. (3)–(6)) will be applied to the simulation of the plastic flow properties in uniaxial tension of polycrystalline materials containing texture components commonly observed experimentally (e.g., see [11]). Specifically, we predict the effect of texture on the variation of the yield stresses $\sigma(\alpha)$ and strain-rate ratios $r(\alpha)$ with the orientation α of the loading axis.

We recall that, by definition, the Lankford coefficient $r(\alpha)$ is the ratio between the in-plane transverse strain-rate, D^p_{22}, and the through-thickness strain-rate, D^p_{33}, under uniaxial loading in a direction at angle α with respect to a reference direction in the plane of the polycrystalline sheet. In the Cartesian frame $(\mathbf{e}_1, \mathbf{e}_2, \mathbf{e}_3)$ associated with the applied loading,

$$r(\alpha) = \frac{D^p_{22}}{D^p_{33}} \tag{7}$$

For all textures, the calculations are done assuming the same set of values for the parameters m_2, n_1, n_3, n_4, c, characterizing the plastic behavior of the constituent crystals (see Eq. (3)). For all textures, the calculations are done assuming the same set of values for the parameters m_2, n_1, n_3, n_4, c, characterizing the plastic behavior of the constituent crystals (see Eq. (3)). These numerical values are: $m_2 = 0.38$, $n_1 = 0.98$, $n_3 = 0.04$, $n_4 = 0.08$, $c = 2.3$, which are representative of aluminum. For more details about the identification procedure based on the uniaxial yield stresses along the crystallographic orientations [100], [111], [110], [211], and [210], the reader is referred to [1].

3. Prediction of the yield stress and Lankford coefficients variation for selected ideal texture components

In polycrystalline metallic sheets, the orientations of the crystals are randomly distributed with high probability densities at a certain number of preferred orientations that result from rotations that occur during processing. The textures that

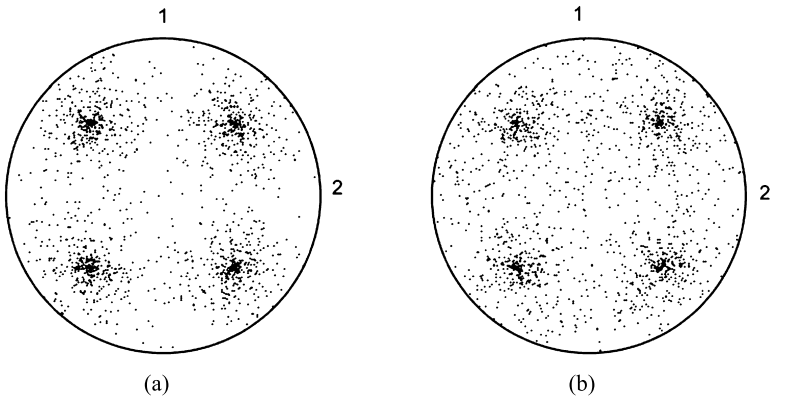

Fig. 1. {111} Pole figures for {100}⟨001⟩ texture corresponding to a series of Gaussian distributions of increasing scatter width: (a) $\omega_0 = 25°$ and (b) $\omega_0 = 35°$.

develop for a given fabrication process are comprised of a relative small number of ideal components (e.g., see [26,11,27]). The ideal texture components that will be considered in this paper are: {100}⟨001⟩ (cube), {110}⟨001⟩ (Goss), {112}⟨111⟩ (copper), and $\{\bar{2}1\bar{1}\}\langle 011\rangle$.

Experimentally, a spread is generally observed around the various ideal texture components. Therefore, following [18,19], a rotationally symmetric Gaussian distribution of misorientations ω_0 about a given ideal orientation will also be considered. The rotation angle ω for the spread is specified as:

$$p(\omega) = p(0)\exp\left(-\frac{1}{2}\omega^2/\omega_0^2\right) \tag{8}$$

For more details about the procedure, the reader is referred to [18,19].

3.1. Cube-textured polycrystalline material

Let us first consider the case of a polycrystalline material containing only the {100}⟨001⟩ (Cube texture) component. For an ideal texture ($\omega_0 = 0°$), the ⟨100⟩ axes of all the constituent crystals are aligned with the texture axes. Under in-plane uniaxial tension, the only non-zero components of the stress, referred to the O*xyz* crystal axes, are: $\sigma_{xx} = \sigma(\alpha)\cos^2\alpha$, $\sigma_{yy} = \sigma(\alpha)\sin^2\alpha$, $\sigma_{xy} = \sigma(\alpha)\sin\alpha\cos\alpha$, with $\sigma(\alpha)$ being the yield stress along the in-plane direction α. The variation of $\sigma(\alpha)$ with the tensile loading orientation can be obtained analytically by substituting the above stresses in the expression (3) of the effective stress associated with the single-crystal yield criterion of [1] as:

$$\frac{\sigma(\alpha)}{\sigma(0)} = \frac{(27 - 4cn_1^2)^{1/6}}{\{27[1 + 3(m_2 - 1)\sin^2\alpha\cos^2\alpha]^3 - c[2n_1 + 9(n_3 - n_1)\sin^2\alpha\cos^2\alpha]^2\}^{1/6}} \tag{9}$$

Likewise, use of Eq. (4) leads to the following expression for the variation of the plastic strain rate ratios $r(\alpha)$ with the loading orientation, α,

$$r(\alpha) = -\frac{\sin^2\alpha\frac{\partial\bar{\sigma}}{\partial\sigma_{xx}} - \sin 2\alpha\frac{\partial\bar{\sigma}}{\partial\sigma_{xy}} + \cos^2\alpha\frac{\partial\bar{\sigma}}{\partial\sigma_{yy}}}{\frac{\partial\bar{\sigma}}{\partial\sigma_{xx}} + \frac{\partial\bar{\sigma}}{\partial\sigma_{yy}}} \tag{10}$$

with $\bar{\sigma}$ being the effective stress given by Eq. (3). Irrespective of the values of the parameters m_2, n_1, n_3, n_4, c, note that the material symmetries are correctly captured. Indeed, Eqs. (9)–(10) predict that the response is identical under rotations of 90° about the normal direction, and in particular: $\sigma(0) = \sigma(90)$ and $r(0) = r(90) = 1$.

For polycrystalline sheets with textures of scatter widths of $\omega_0 = 25°$ and $\omega_0 = 35°$ from the ideal {100}⟨001⟩ cube texture, simulations were done using the polycrystal model (Eqs. (3)–(6)) for samples of 400 crystals. As an example, in Fig. 1 are shown the {111} pole figures for the textures considered (see also Eq. (8)). The evolution of yield stress ratios $\sigma(\alpha)/\sigma(0)$ and Lankford coefficients $r(\alpha)$ with the loading direction α for these cube-textured sheets according to the polycrystal model with the given values for the parameters describing the constituent grain behavior ($m_2 = 0.38$, $n_1 = 0.98$, $n_3 = 0.04$, $n_4 = 0.08$, $c = 2.3$) is shown in Fig. 2. In Fig. 2 are also plotted the analytical predictions for the ideal cube texture ($\omega_0 = 0°$) calculated using Eqs. (9)–(10).

Note that, irrespective of the scatter width ω_0 about the ideal texture, both the predicted macroscopic yield stresses and r-values vary smoothly with the loading orientation (see Fig. 2). Additionally, irrespective of ω_0, for the given values of the parameters characterizing the behavior of the grains, minima in yield stresses are along the 0° and 90° orientations and there is only one peak which corresponds to uniaxial loading at 45°. The predicted variation of the Lankford coefficients with

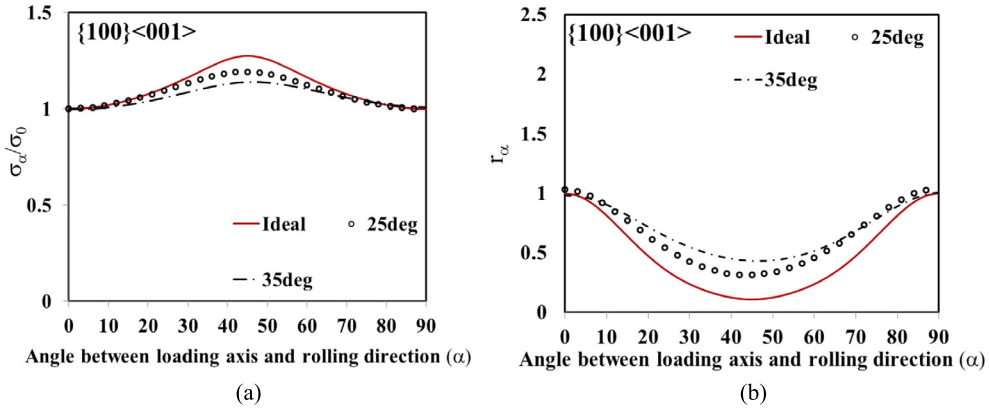

Fig. 2. Numerical simulations, using the new polycrystal model, of the anisotropy in: (a) yield stress ratio $\sigma(\alpha)$ and (b) strain-ratio $r(\alpha)$ in the plane of the $\{100\}\langle 001\rangle$ textured polycrystalline sheet. The textures for different scatter width ω_0 are shown in Fig. 1. The results for the ideal texture were obtained with the analytical formulas (Eqs. (9)–(10)), respectively.

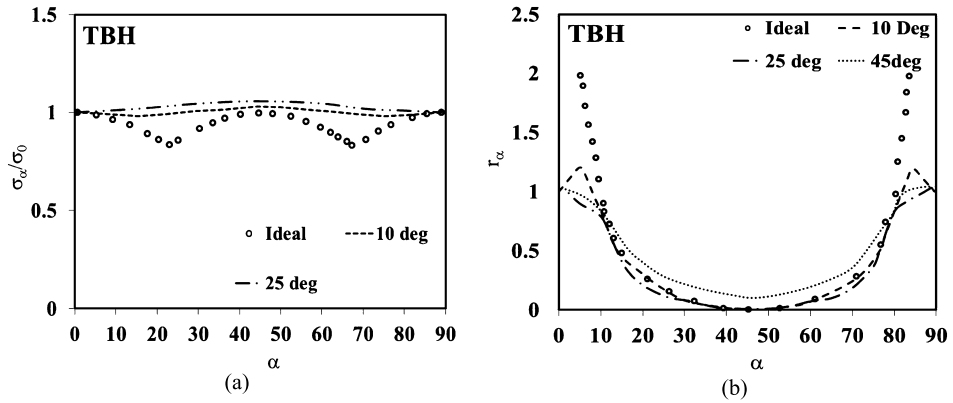

Fig. 3. Effect of initial texture on the anisotropy in: (a) yield stress ratio and (b) strain ratio in the plane of the polycrystalline cube-textured sheet using the Taylor–Bishop–Hill approach (after [18]).

the orientation is such that there is only one minimum corresponding to uniaxial tension along the 45° in-plane direction. Note also, that for the rotationally symmetric Gaussian distribution of misorientations with $\omega_0 = 25°$ and $\omega_0 = 35°$, the directional dependence of the macroscopic plastic properties in the plane of the sheet is similar to that predicted analytically for an ideal texture, but the anisotropy is less pronounced.

It is well documented that for an ideal ($\omega_0 = 0°$) $\{100\}\langle 001\rangle$ texture the yield stress variation with the loading orientation according to the TBH model displays two cusps, while the Lankford coefficients are not defined for the 0° and 90° tensile loadings (e.g., see [18]), i.e. $r(0°)$ and $r(90°)$ have infinite values. Additionally, for that model, only when the texture is characterized by a larger spread, the predicted variation in both the macroscopic yield stresses and Lankford coefficients is smooth (see Fig. 3, after [18,19]).

3.2. *Goss texture* $\{110\}\langle 001\rangle$

For an ideal $\{110\}\langle 001\rangle$ textured sheet (Goss texture), using the single-crystal yield criterion of [1], an analytic formula for the evolution of the uniaxial yield stress ratio $\sigma(\alpha)/\sigma(0)$ with the loading direction α in the plane of the sheet can be obtained by referring the applied stress tensor to the crystal axes and further substituting the respective components in Eq. (3). The variation of the tensile yield stresses as a function of the loading direction α and the coefficients m_2, n_1, n_3, n_4, c is:

$$\frac{\sigma(\alpha)}{\sigma(0)} = \frac{2(27 - 4cn_1^2)^{1/6}}{\left\{ \begin{array}{l} [12 + 9(m_2 - 1)(1 + 3\cos^2\alpha)\sin^2\alpha]^3 \\ -c[16n_1 + 54(n_1 - 3n_3 + 2n_4)\sin^4\alpha\cos^2\alpha + 18(n_3 - n_1)\sin^2\alpha(1 + 3\cos^2\alpha)]^2 \end{array} \right\}^{1/6}} \tag{11}$$

Likewise, the variation of the plastic strain-rate ratios $r(\alpha)$ with the orientation α can also be obtained analytically as a function of the coefficients m_2, n_1, n_3, n_4, c by making use of Eq. (4):

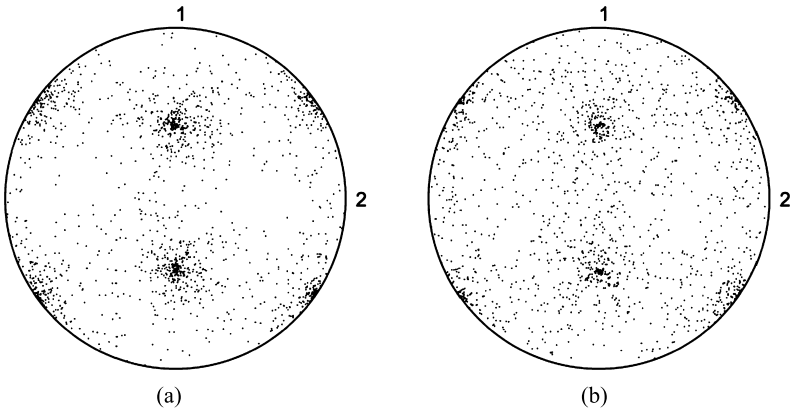

Fig. 4. {111} Pole figures for the {110}⟨001⟩ texture corresponding to a series of Gaussian distributions of increasing scatter width: (a) $\omega_0 = 25°$ and (b) $\omega_0 = 35°$.

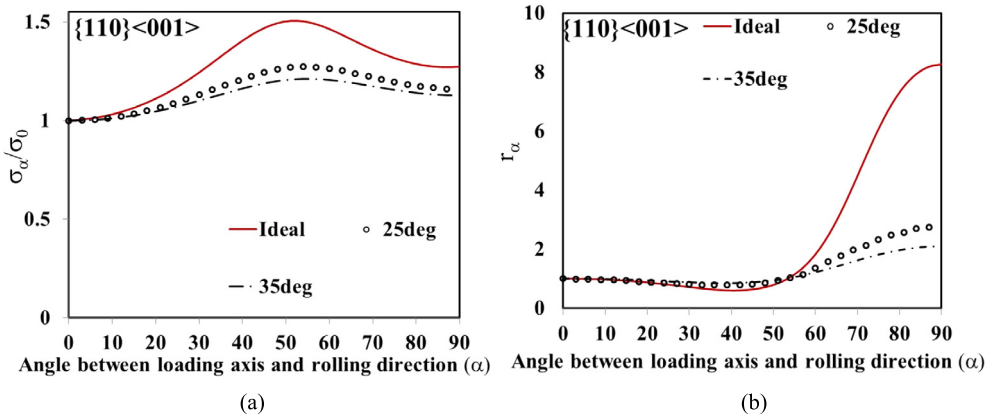

Fig. 5. Numerical simulations, using the new polycrystal model, of the anisotropy in (a) yield stress ratio $\sigma(\alpha)$ and (b) strain ratio $r(\alpha)$ in the plane of the {110}⟨001⟩ textured polycrystalline sheet. The textures for different scatter width ω_0 are shown in Fig. 4. The results for the ideal texture were obtained with the analytical formulas (Eqs. (11)–(12)), respectively.

$$r(\alpha) = \frac{(3\cos^2\alpha - 2)\left(\frac{\partial\bar{\sigma}}{\partial\sigma_{xx}} + \frac{\partial\bar{\sigma}}{\partial\sigma_{yy}}\right) - 2\cos^2\alpha\,\frac{\partial\bar{\sigma}}{\partial\sigma_{xy}} - \sqrt{2}\sin(2\alpha)\,\frac{\partial\bar{\sigma}}{\partial\sigma_{xz}}}{\frac{\partial\bar{\sigma}}{\partial\sigma_{xx}} + \frac{\partial\bar{\sigma}}{\partial\sigma_{yy}} + 2\frac{\partial\bar{\sigma}}{\partial\sigma_{xy}}} \tag{12}$$

where $\bar{\sigma}$ is the plastic potential given by Eq. (3) and its derivatives are expressed in terms of the stress components in the crystal axes. Note that irrespective of the values of the parameters m_2, n_1, n_3, n_4, c, the model correctly accounts for the material symmetries, namely that $r(0) = 1$. In Fig. 5 are shown the predicted variations of macroscopic plastic properties with the loading orientation according to the analytical formulas (11)–(12) for the given textures (the {111} pole figures are shown in Fig. 4). The effect of texture, namely of the spread ω_0 with respect to the ideal Goss texture, on the directional dependence of the same macroscopic properties (yield stresses, plastic strain ratios) simulated with the polycrystalline model are plotted on the same figure for comparison. For the texture obtained from rotationally symmetric Gaussian distribution of misorientation with ω_0 up to 35°, the anisotropy in $\sigma(\alpha)/\sigma(0)$ vs. α and $r(\alpha)$ vs. α variations are much less pronounced than the respective curves for the ideal Goss texture For example, for $\omega_0 = 35°$ the value of $r(90°)$ is about five times smaller than that for $\omega_0 = 0$). Nevertheless, the nature of the $r(\alpha)$ variation is similar irrespective of the spread, with a point of inflection at around 55° from the reference direction (see Fig. 5).

It is also worth noting that the use of our polycrystalline model leads to finite values for the Lankford coefficients irrespective of the in-plane loading direction. This is not the case if the TBH model is applied. It is well documented (e.g., see [28]) that in order to obtain with the TBH model a smooth variation in r-values in the polycrystalline sample a large percentage of the grains should be taken with random orientations. For example, by considering as much as 50% of the total volume fraction of grains having isotropic orientations and 50% having almost ideal texture (i.e. spread around ideal texture very small, ∼5°), Barlat and Richmond [28] obtained a smooth variation of the r-values with the loading direction. However, the predicted $r(\alpha)$ vs. α curve has a vertical asymptote at $\alpha \cong 70°$. As concerns the predictions of our model in terms of yield stress anisotropy, the absolute maximum in yield stresses is at a loading orientation of ∼55°. Note that this holds true for both the ideal Goss texture and for rotationally symmetric texture with scatter widths of $\omega_0 = 25°$ and $\omega_0 = 35°$.

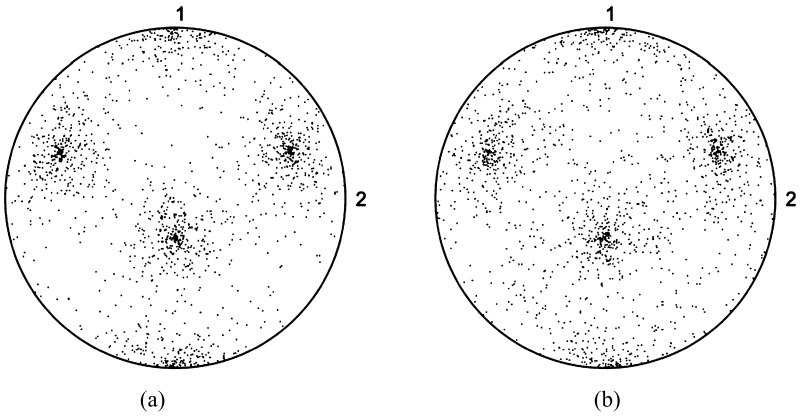

Fig. 6. {111} Pole figures for the $\{112\}\langle 1\bar{1}\bar{1}\rangle$ texture corresponding to a series of Gaussian distributions of increasing scatter width: (a) $\omega_0 = 25°$ and (b) $\omega_0 = 35°$.

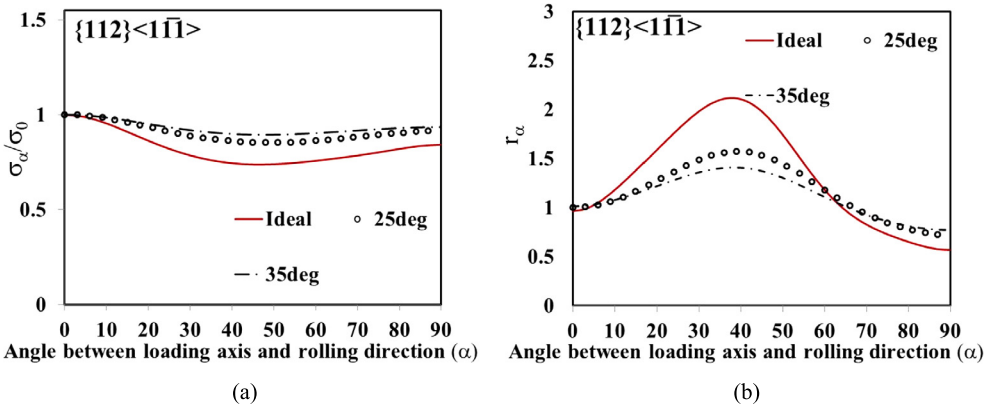

Fig. 7. Numerical simulations, using the new polycrystal model, of the anisotropy in (a) yield stress ratio $\sigma(\alpha)$ and (b) strain ratio $r(\alpha)$ in the plane of the $\{112\}\langle 1\bar{1}\bar{1}\rangle$ textured polycrystalline sheet. The textures for different scatter width ω_0 are shown in Fig. 6. The results for ideal texture were obtained with the analytical formulas (Eqs. (13)–(14)), respectively.

3.3. *Copper texture* $\{112\}\langle 11\bar{1}\rangle$

For an ideal $\{112\}\langle 11\bar{1}\rangle$ textured sheet (copper texture), an analytic formula for the variation of the uniaxial yield stress ratio $\sigma(\alpha)/\sigma(0)$ with the loading direction α in the plane of the sheet can be obtained by referring the applied stress tensor to the crystal axes and further substituting the respective components in Eq. (3):

$$\frac{\sigma(\alpha)}{\sigma(0)} = \frac{2(27 - 4cn_1^2)^{1/6}}{\left\{\begin{array}{l}[12 + 3(m_2 - 1)(4\cos^4\alpha + 3\sin^4\alpha)]^3 \\ -c[16n_1 + 2(n_1 - 3n_3 + 2n_4)\sin^2\alpha(5\sin^2\alpha - 2) + 6(n_3 - n_1)(4\cos^4\alpha + 3\sin^4\alpha)]^2\end{array}\right\}^{1/6}} \tag{13}$$

Similarly, the dependence of the plastic strain-rate ratios $r(\alpha)$ with the loading orientation α can also be obtained analytically as a function of the coefficients m_2, n_1, n_3, n_4, c characterizing the constituent crystals plastic behavior.

$$r(\alpha) = \frac{\left[\begin{array}{l}-3\cos^2\alpha\frac{\partial\bar{\sigma}}{\partial\sigma_{zz}} + \sqrt{6}\sin 2\alpha(\frac{\partial\bar{\sigma}}{\partial\sigma_{xx}} - \frac{\partial\bar{\sigma}}{\partial\sigma_{yy}}) - 4\sin^2\alpha(\frac{\partial\bar{\sigma}}{\partial\sigma_{yz}} + \frac{\partial\bar{\sigma}}{\partial\sigma_{xz}}) \\ + \sqrt{6}\sin 2\alpha(\frac{\partial\bar{\sigma}}{\partial\sigma_{yz}} - \frac{\partial\bar{\sigma}}{\partial\sigma_{xz}}) - 2(5\cos^2\alpha - 2)\frac{\partial\bar{\sigma}}{\partial\sigma_{xy}}\end{array}\right]}{3(\frac{\partial\bar{\sigma}}{\partial\sigma_{zz}}) + 2(\frac{\partial\bar{\sigma}}{\partial\sigma_{xy}} + 2\frac{\partial\bar{\sigma}}{\partial\sigma_{xz}} + 2\frac{\partial\bar{\sigma}}{\partial\sigma_{yz}})} \tag{14}$$

For the given set of numerical values of these parameters, the predicted variation is shown in Fig. 7. For textures with spreads $\omega_0 = 25°$ and $\omega_0 = 35°$ (see Fig. 6 for the {111} pole figures), the trends in the directional dependence of the macroscopic plastic properties is similar to the ideal orientation case. Irrespective of the spread, the maximum value for the Lankford coefficients is obtained in uniaxial tension at an orientation $\alpha \cong 39°$ from the reference direction, while the maximum uniaxial yield stress is at $\alpha = 0$.

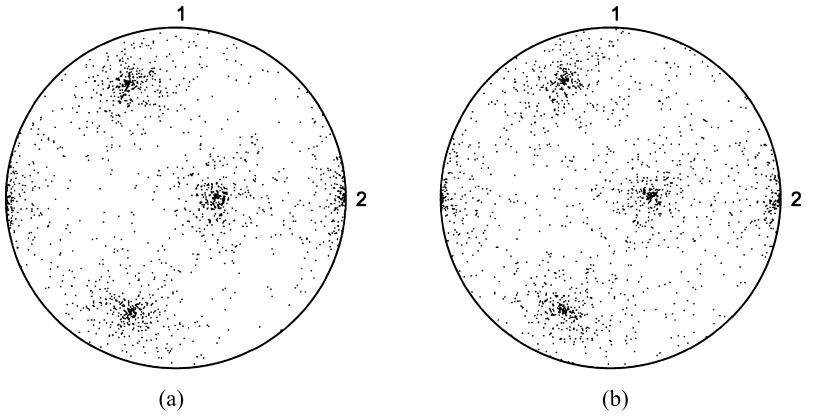

Fig. 8. {111} Pole figures for the $\{\bar{2}1\bar{1}\}\langle 011\rangle$ texture corresponding to a series of Gaussian distributions of increasing scatter width: (a) $\omega_0 = 25°$ and (b) $\omega_0 = 35°$.

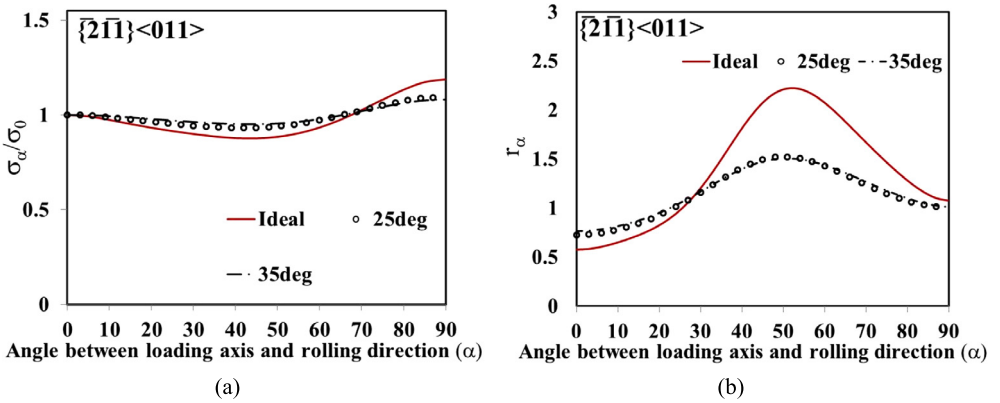

Fig. 9. Numerical simulations, using the new polycrystal model, of the anisotropy in (a) yield stress ratio $\sigma(\alpha)$ and (b) strain ratio $r(\alpha)$ in the plane of the $\{2\bar{1}\bar{1}\}\langle 011\rangle$ textured polycrystalline sheet. The textures for different scatter width ω_0 are shown in Fig. 8. The results for ideal texture were obtained with the analytical formulas (Eqs. (15)–(16)), respectively.

3.4. $\{\bar{2}1\bar{1}\}\langle 011\rangle$ *texture component*

For an ideal texture $\{\bar{2}1\bar{1}\}\langle 011\rangle$, using the same criterion given by Eq. (1) for the description of the plastic deformation of each grain, under uniaxial tension along an axis at orientation α, the yield stress is:

$$\frac{\sigma(\alpha)}{\sigma(0)} = \frac{[(9m_2+3)^3 - 256cn_1^2]^{1/6}}{\left\{\begin{array}{l}[12+3(m_2-1)(3\cos^4\alpha+4\sin^4\alpha)]^3 \\ -c[16n_1+2(n_1-3n_3+2n_4)(5\cos^2\alpha-2)\sin^2\alpha+6(n_3-n_1)(3\cos^4\alpha+4\sin^4\alpha)]^2\end{array}\right\}^{1/6}} \tag{15}$$

The variation of the Lankford coefficients with the loading orientation α is given by:

$$r(\alpha) = \frac{\left[\begin{array}{l}-(3\sin^2\alpha+\sqrt{6}\sin 2\alpha)\frac{\partial\bar{\sigma}}{\partial\sigma_{xx}} - 2\sqrt{6}\sin 2\alpha\frac{\partial\bar{\sigma}}{\partial\sigma_{yy}} + (1-5\cos 2\alpha)\frac{\partial\bar{\sigma}}{\partial\sigma_{yz}} \\ +4\cos^2\alpha(\frac{\partial\bar{\sigma}}{\partial\sigma_{xy}} - \frac{\partial\bar{\sigma}}{\partial\sigma_{xz}}) - \sqrt{6}\sin 2\alpha(\frac{\partial\bar{\sigma}}{\partial\sigma_{xy}} + \frac{\partial\bar{\sigma}}{\partial\sigma_{xz}})\end{array}\right]}{[3(\frac{\partial\bar{\sigma}}{\partial\sigma_{xx}}) + 2(\frac{\partial\bar{\sigma}}{\partial\sigma_{xz}} - \frac{\partial\bar{\sigma}}{\partial\sigma_{xy}} - \frac{\partial\bar{\sigma}}{\partial\sigma_{yz}})]} \tag{16}$$

In the above expression, $\bar{\sigma}$ is given by Eq. (3), and its derivatives are expressed in terms of the stress components in the crystal axes.

In Fig. 9 are shown the predicted macroscopic mechanical properties in uniaxial tension for the material with ideal texture calculated using the analytical formulas (Eq. (15)–(16)) and the polycrystalline simulation results for the textures corresponding to Gaussian distributions of scatter width of $\omega_0 = 25°$ and 35° with respect to the ideal $\{\bar{2}1\bar{1}\}\langle 011\rangle$ texture (see Fig. 8 for the {111} pole figures of these textures).

First, let us note that irrespective for $\omega_0 = 25°$ and $\omega_0 = 35°$, it is predicted a very moderate anisotropy in yield stresses, the variation of the yield stresses with the loading orientation being almost the same, with a minimum at $\alpha \cong 45°$ load-

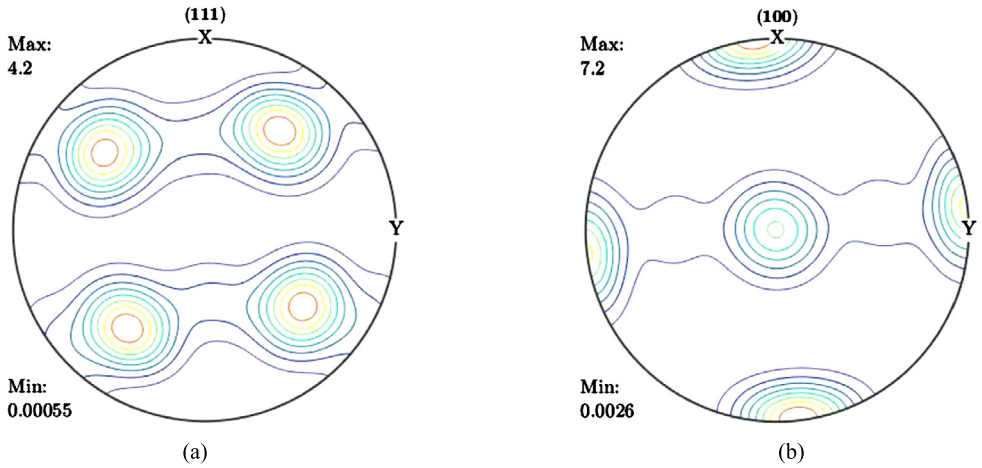

Fig. 10. Pole figures for a sheet with a mixture of {100}⟨001⟩ component (80%) and {110}⟨001⟩ component (20%) (a) {111} (b) {100}.

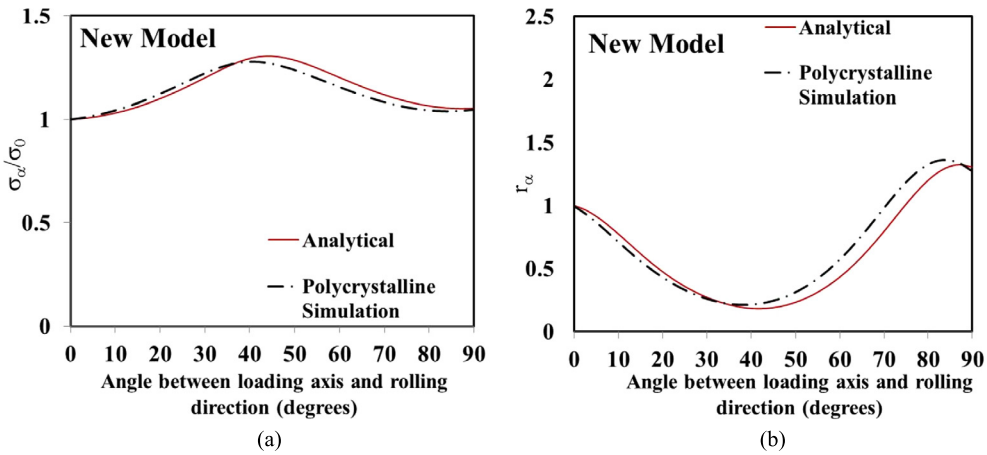

Fig. 11. Numerical simulations of anisotropy in (a) yield stress ratio and (b) strain ratio in the plane of the polycrystalline sheet predicted by the new polycrystal model for a strongly textured polycrystal with components spread around the {100}⟨001⟩(80%) and {110}⟨001⟩(20%) orientations. The texture is shown in Fig. 10.

ing orientation, and a maximum at $\alpha = 90°$. As concerns the predicted anisotropy in Lankford coefficients (see Fig. 9b), irrespective of ω_0 the trends are the same, the anisotropy becoming less pronounced as the width spread ω_0 increases.

In summary, irrespective of the texture component considered, the analytical formulas provide a very good estimate of the trend in anisotropy in macroscopic plastic properties. Next, using the new yield criterion [1] (see Eq. (1)) for the description of the plastic behavior of the constituent grains, we will investigate the predicted mechanical response of strongly textured polycrystalline materials containing various combinations of ideal texture components.

4. Predictions of anisotropy of yield stresses and Lankford coefficients for textured sheets containing several components

It is of fundamental importance to predict the manner in which a given texture component affects the plastic anisotropy of the polycrystal. To this end, we will analyze model materials containing a combination of two of the texture components commonly observed in real materials.

Let us first consider a polycrystalline sheet with components spread ($\omega_0 = 5°$) around the {100}⟨001⟩ (80% volume fraction) and {110}⟨001⟩ (20% volume fraction), respectively. The texture of the polycrystalline sheet is shown in Fig. 10.

In Fig. 11 are shown the macroscopic yield stress and plastic strain ratios obtained by using the analytical formulas for {100}⟨001⟩ (Eqs. (9)–(10)) and {110}⟨001⟩ ideal textures (Eqs. (11)–(12)) in conjunction with simple laws of mixtures. Specifically, the yield stress of the polycrystal is calculated as a weighted mean using Eq. (9) and Eq. (11), respectively. As concerns, the r-value calculation, it is done by weighting the strain-rates corresponding to each texture component, i.e.:

$$r(\alpha) = -\frac{f_1[\sin^2\alpha\,\frac{\partial\bar{\sigma}^{(1)}}{\partial\sigma_{xx}} - \sin 2\alpha\,\frac{\partial\bar{\sigma}^{(1)}}{\partial\sigma_{xy}} + \cos^2\alpha\,\frac{\partial\bar{\sigma}^{(1)}}{\partial\sigma_{yy}}] + f_2[\sin^2\alpha\,\frac{\partial\bar{\sigma}^{(2)}}{\partial\sigma_{xx}} - \sin 2\alpha\,\frac{\partial\bar{\sigma}^{(2)}}{\partial\sigma_{xy}} + \cos^2\alpha\,\frac{\partial\bar{\sigma}^{(2)}}{\partial\sigma_{yy}}]}{f_1(\frac{\partial\bar{\sigma}^{(1)}}{\partial\sigma_{xx}} + \frac{\partial\bar{\sigma}^{(1)}}{\partial\sigma_{yy}}) + f_2(\frac{\partial\bar{\sigma}^{(2)}}{\partial\sigma_{xx}} + \frac{\partial\bar{\sigma}^{(2)}}{\partial\sigma_{yy}})}$$

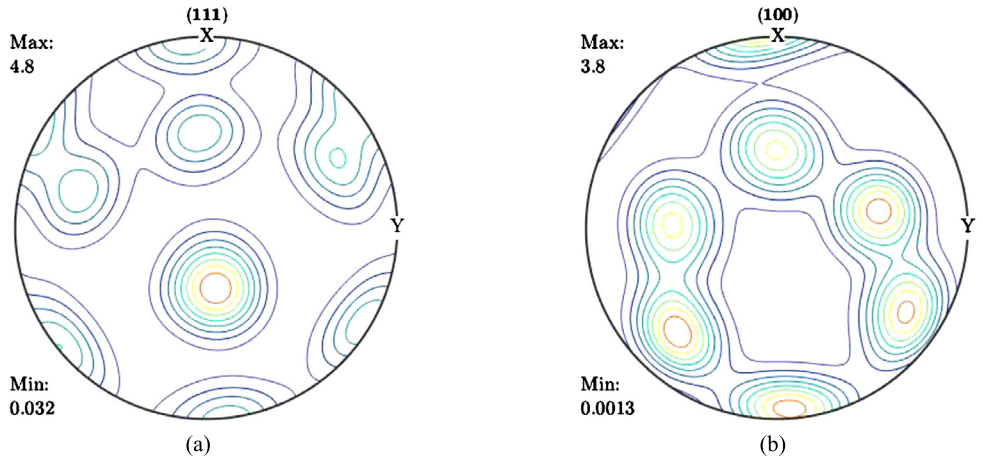

Fig. 12. Pole figures for a sheet with a mixture of $\{112\}\langle 1\overline{1}1\rangle$ components (50%) and $\{110\}\langle 001\rangle$ component (50%) (a) {111} and (b) {100}.

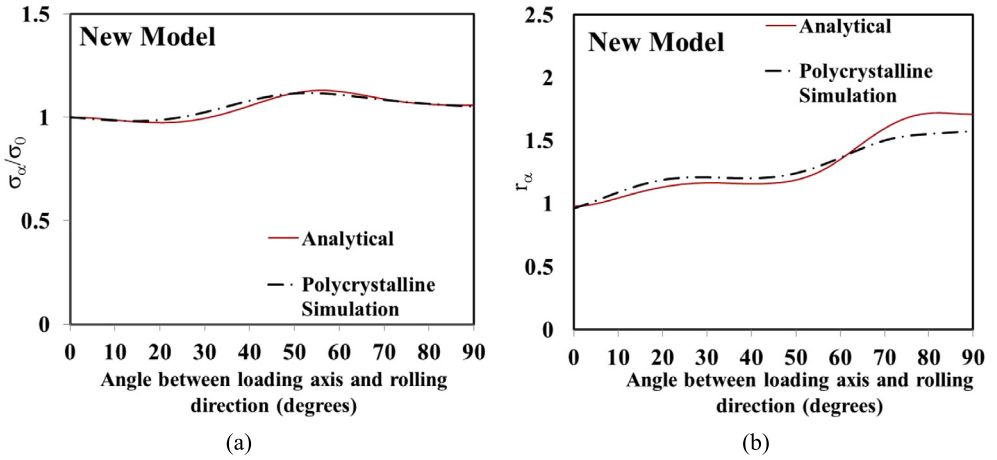

Fig. 13. Numerical simulations of anisotropy in (a) yield stress ratio and (b) strain ratio in the plane of the polycrystalline sheet predicted by the new polycrystal model for a strongly textured polycrystal with components spread around the $\{112\}\langle 1\overline{1}1\rangle$(50%) and $\{110\}\langle 001\rangle$(50%) orientations. The texture is shown in Fig. 12.

In the above equation, $\bar{\sigma}^{(1)}$ and $\bar{\sigma}^{(2)}$ are the effective stress corresponding to the respective texture component calculated using Eq. (3); all the derivatives are expressed in terms of stress components in the [100] axes; f_1 and f_2 are the weights of each component.

On the other hand, in the numerical predictions, we used 400 grains in the sample and we accounted for a small statistical misorientation ($\omega_0 = 5°$) about the ideal textures. The overall response was numerically assessed using the single-crystal yield criterion and associated flow rule.

Note that the analytical estimates are very close to the numerical results obtained using the same criterion (i.e. [1]) for the description of the plastic behavior of the constituent grains. The shapes of both the $\sigma(\alpha)/\sigma(0)$ and $r(\alpha)$ curves are similar to those corresponding to the cube texture (compare Fig. 11 with Fig. 2). However, the presence of the Goss component (20% volume fraction) results in $r(90°)$ larger than $r(0°)$ and the minimum r-value is slightly larger than in the case of the ideal cube texture. Specifically, for the given values of the coefficients characterizing the behavior of the constituent grains, $r(90°) = 1.27 > r(0°) = 1$ and the minimum r-value corresponds to tensile loading along a direction $\alpha = 39°$. Note also that $r(39°) = 0.21$, which is double the minimum r-value for an ideal cube texture (see Fig. 2b; the minimum is $r(45°) = 0.1$).

For a polycrystalline sheet with texture containing copper and Goss components in the same proportion (see pole figures in Fig. 12), the results of the polycrystalline numerical simulations and analytical estimates obtained using the formulas for each ideal texture component in conjunction with the respective laws of mixtures are shown in Fig. 13. Note that the analytical predictions are very close to the numerical predictions.

It is interesting to note that the predicted $\sigma(\alpha)/\sigma(0)$ curve is almost flat indicating little variation in yield stresses for loading orientation α between 0° and 20°, the anisotropy becoming slightly more pronounced for loading directions between 20° and 70°, with a peak in yield stress around 50°, and very little difference between yield stresses for loadings

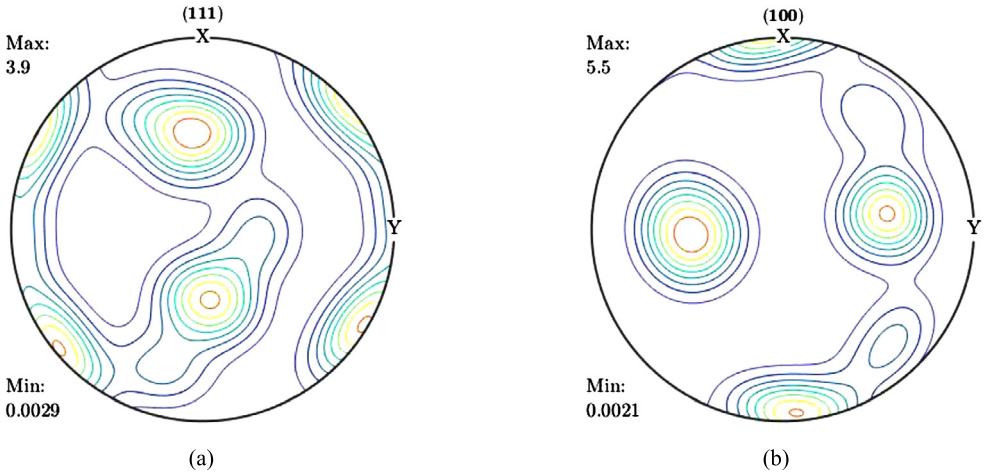

Fig. 14. Pole figures for a sheet with a mixture of $\{\bar{2}\bar{1}\bar{1}\}\langle 011\rangle$ components (30%) and $\{110\}\langle 001\rangle$(70%) component (70%) (a) {111} and (b) {100}.

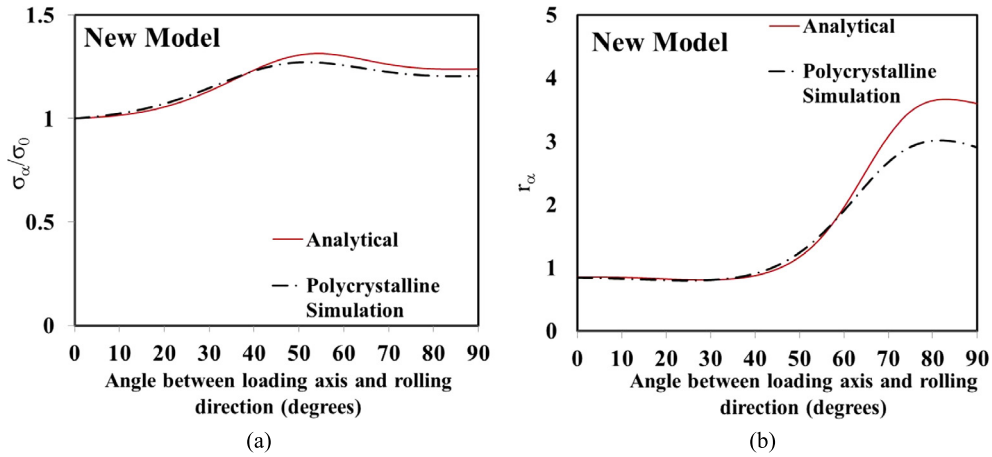

Fig. 15. Numerical simulations of anisotropy in (a) yield stress ratio and (b) strain ratio in the plane of the polycrystalline sheet predicted by the new polycrystal model for a strongly textured polycrystal with components spread around the $\{\bar{2}\bar{1}\bar{1}\}\langle 011\rangle$(30%) and $\{110\}\langle 001\rangle$(70%) orientations. The texture is shown in Fig. 14.

between 70° and 90°. While the shape of the $\sigma(\alpha)/\sigma(0)$ curve is concave down, thus closer to that of the ideal Goss component (see also Fig. 5a), the anisotropy is much less pronounced and similar to that of the ideal copper component (compare with Fig. 7). It is interesting to note that $r(0°) = 1$ as it is the case for an ideal Goss component, and in the $r(\alpha)$ vs. α curve there is an inflexion point between 40° and 50°, also observed in the r-value variation for an ideal Goss component (see Fig. 5b). However, the r-value predicted for tensile loading at $\alpha = 90°$ is much lower. The presence of the copper component in the texture, lowers the $r(90°)$ value from about $r(90°) \sim 8$, in the case of an ideal Goss component (see Fig. 5b), to $r(90°) = 1.57$.

Next, we consider a polycrystalline sheet with texture shown in Fig. 14. While the dominant texture component (70% volume fraction) has a spread ($\omega_0 = 5°$) about $\{110\}\langle 001\rangle$ Goss texture, the texture also contains a component with spread ($\omega_0 = 5°$) about $\{\bar{2}1\bar{1}\}\langle 011\rangle$ (30% volume fraction). Fig. 15 presents the predicted evolution of the macroscopic yield stresses and plastic strain ratios for this material obtained on the basis of the same yield criterion for the constituent grains, i.e. the analytical estimate (based on the analytical formulas for each ideal component present in the texture) and the results of polycrystalline simulations. The analytical $\sigma(\alpha)/\sigma(0)$ vs. α variation is very close to the numerical one. The analytical $r(\alpha)$ vs. α and the polycrystalline simulation results are similar with $r(0°) = 1$, very little variation in r-values for loading orientations α between 0° and 40°, inflection point at $\alpha \sim 45°$ and a sharp upward trend as in the case of the ideal Goss component (note that the point of inflection was $\alpha = 39°$ for ideal Goss orientation). It is to be noted that although analytically a higher r-value is predicted in the transverse direction ($\alpha = 90°$) than the numerically predicted value, the analytical estimate captures the influence of the $\{\bar{2}1\bar{1}\}\langle 011\rangle$ component. Namely, it predicts that the $\{\bar{2}1\bar{1}\}\langle 011\rangle$ component contributes to a significant decrease in anisotropy of the material. For example, the predicted r-value in the transverse direction is significantly lower than that predicted for the ideal Goss component (compare Fig. 15b with Fig. 5b).

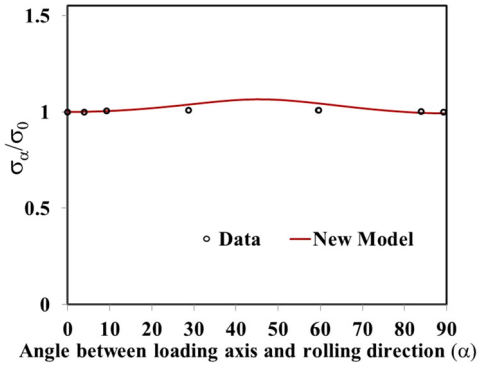

Fig. 16. Comparison between the experimental yield stress ratio in the plane of a 10% rolled annealed polycrystalline Al sheet and the numerical simulations using the new polycrystal model. Data after [24].

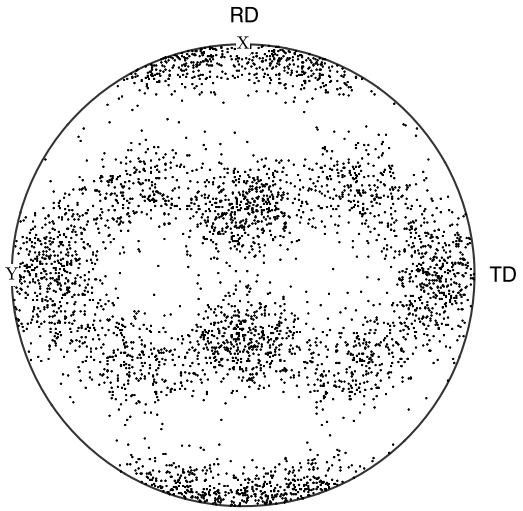

Fig. 17. {111} Pole figure for an AA 2024-T3 aluminum sheet.

Finally, the proposed polycrystalline model is applied to aluminum-based polycrystalline sheets. The first example concerns a pure aluminum sheet (data after [24]). It was reported that 60% of the total volume fraction of grains have isotropic orientations while 40% have $\{100\}\langle 001\rangle$ orientation. Simulation results of the variation in yield stresses with the orientation of the tensile loading direction performed using the proposed polycrystalline model (Eqs. (3)–(6)) are shown in Fig. 16. It is predicted a smooth variation with the in-plane orientation, with a peak at 45° to the rolling direction (characteristic of the ideal cube texture, see also Fig. 2a). However, the presence of the random texture component contributes to a significant decrease in anisotropy. A good agreement between the simulated and experimentally measured stress ratios is obtained.

The last example, concerns a 2024-T3 aluminum alloy sheet (data after [25]). Fig. 17 shows the {111} pole figure with 1000 discretized crystallite orientations while in Fig. 18 is presented a comparison between the experimental and predicted variation of the Lankford coefficients with the tensile loading orientation obtained using the new polycrystalline model (with the same values for the m_2, n_1, n_3, n_4, c coefficients characterizing the constituent crystals plastic behavior: $m_2 = 0.38$, $n_1 = 0.98$, $n_3 = 0.04$, $n_4 = 0.08$, $c = 2.3$), and the TBH model, respectively. To obtain the r-values according to the TBH model, we used the LApp (Los Alamos polycrystal plasticity) code developed by [29]. Note that the new model is in good quantitative agreement with the experimental r-values. The fact that the TBH model largely overpredicts the experimental r-values is not surprising, because it is well documented in the literature that this theory does not fare well with the experimental Lankford coefficients for aluminum alloys (see for example, [30,31] for 2008-T4 series aluminum alloy; [4] for a 6000 series aluminum alloy).

5. Conclusions

Using a new constitutive model developed by [1] for the description of the individual constituent grains, the effect of texture on uniaxial plastic properties of polycrystalline materials has been investigated. This single-crystal yield criterion is expressed in terms of generalized stress invariants and as such automatically satisfies the intrinsic crystal symmetries. It is represented by a function C^2 differentiable for any three-dimensional loadings. Therefore, for ideal texture components, it

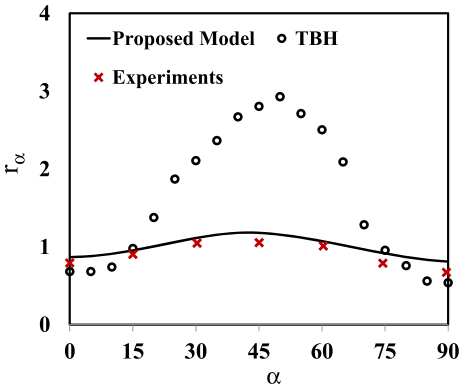

Fig. 18. Comparison of experimental and predicted anisotropy in *r*-values according to the proposed new polycrystal model and the TBH model obtained for AA 2024-T3 (data after [25]). TBH model predictions are obtained with the code LApp [29].

is possible to derive analytic formulas for the variation of the macroscopic yield stress and Lankford coefficients with the in-plane loading direction.

For the case of strongly textured materials with a distribution of grain orientations with various spreads about the ideal texture components, the anisotropy of the polycrystalline response is simulated numerically assuming uniform stress in each grain and the same single crystal criterion for the description of the behavior of the constituent grains. An added advantage is that irrespective of the number of grains in the sample, Lankford coefficients have finite values for all loading orientations even for ideal texture components, i.e. there is no need to add random texture components to gauge the plastic properties of the polycrystal. Moreover, for textured materials with rotationally symmetric grain orientations spread around one ideal texture component $\omega_0 \leq 35°$, the simulation results of anisotropy in polycrystalline response obtained with samples of 400 grains are much less pronounced but still similar in nature to those obtained analytically. Irrespective of the texture component considered, the analytical formulas provide a good estimate of the in-plane anisotropy and its trends at a very low calculation cost.

When more than one ideal texture component exists in the material, polycrystalline simulations based on the new description of the plastic behavior of the constituent grains capture the influence of individual texture components on the overall plastic anisotropy of the polycrystal. Additionally, it was shown that the use of the analytical formulas for each ideal component in conjunction with laws of mixtures provides an adequate estimate of the in-plane anisotropy. Therefore, the trends in plastic anisotropy of the macroscopic properties, and most importantly how the predominant texture components affect the deformation can be adequately estimated analytically using the described approach. Finally, the good agreement between the experimental and theoretical predictions of the anisotropy in *r*-values obtained with the new polycrystalline model for 2024-T3 aluminum alloy sheet (data after [25]) demonstrates the predictive capabilities of the new polycrystalline model.

References

[1] O. Cazacu, B. Revil-Baudard, N. Chandola, A yield criterion for cubic single crystals, Int. J. Solids Struct. (2017), https://doi.org/10.1016/j.ijsolstr.2017.04.006.
[2] R. Hill, A theory of the yielding and plastic flow of anisotropic metals, Proc. R. Soc. Lond. A, Math. Phys. Eng. Sci. 193 (1948) 281–297.
[3] O. Cazacu, F. Barlat, Generalization of Drucker's yield criterion to orthotropy, Math. Mech. Solids 6 (2001) 613–630.
[4] O. Cazacu, F. Barlat, Application of the theory of representation to describe yielding of anisotropic aluminum alloys, Int. J. Eng. Sci. (2003) 1367–1385.
[5] O. Cazacu, F. Barlat, A criterion for description of anisotropy and yield differential effects in pressure-insensitive metals, Int. J. Plast. 20 (2004) 2027–2045.
[6] F. Barlat, H. Aretz, J.W. Yoon, M.E. Karabin, J.C. Brem, R.E. Dick, Linear transformation-based anisotropic yield functions, Int. J. Plast. 21 (2005) 1009–1039.
[7] M.E. Nixon, O. Cazacu, R.A. Lebensohn, Anisotropic response of high-purity α-titanium: experimental characterization and constitutive modeling, Int. J. Plast. 26 (2010) 516–532.
[8] G.I. Taylor, Analysis of plastic strain in a cubic crystal, in: Stephen Timoshenko 60th Anniversary Volume, 1938, pp. 218–224.
[9] J.F.W. Bishop, R. Hill, A theoretical derivation of the plastic properties of a polycrystalline face-centered metal, London, Edinburgh, Dublin Philos. Mag. J. Sci. 42 (334) (1951) 1298–1307.
[10] J.F.W. Bishop, R. Hill, A theory of the plastic distortion of a polycrystalline aggregate under combined stresses, London, Edinburgh, Dublin Philos. Mag. J. Sci. 42 (334) (1951) 414.
[11] U.F. Kocks, C.N. Tomé, H.R. Wenk, Texture and Anisotropy: Preferred Orientations in Polycrystals and Their Effect on Materials Properties, Cambridge University Press, 2000.
[12] P. Van Houtte, S. Li, O. Engler, Taylor-type homogenization methods for texture and anisotropy, in: D. Raabe, L.Q. Chen, F. Barlat, F. Roters (Eds.), Continuum Scale Simulation of Engineering Materials, Fundamentals – Microstructures – Process Applications, Wiley, Berlin, 2004, pp. 459–471.
[13] C.N. Tomé, R.A. Lebensohn, Self-consistent homogenization methods for texture and anisotropy, in: D. Raabe, L.Q. Chen, F. Barlat, F. Roters (Eds.), Continuum Scale Simulation of Engineering Materials, Fundamentals – Microstructures – Process Applications, Wiley, Berlin, 2004, pp. 473–499.
[14] P. Eyckens, H. Mulder, J. Gawad, H. Vegter, D. Roose, T. van den Boogaard, A. Van Bael, P. Van Houtte, Int. J. Plast. 73 (2015) 119–141.
[15] M. Arminjon, A regular form of the Schmid law. Application to the ambiguity problem, Textures Microstruct. 14 (1991) 1121–1128.

[16] H.C.H. Carpenter, C.F. Elam, The production of single crystals of aluminum and their tensile properties, Proc. R. Soc. Lond., Ser. A 704 (1921) 329–353.
[17] G.E.G. Tucker, Texture and earing in deep drawing of aluminium, Acta Metall. 9 (1961) 275–286.
[18] P.H. Lequeu, P. Gillormini, F. Montheillet, B. Bacroix, J.J. Jonas, Yield surfaces for textured polycrystals – I. Crystallographic approach, Acta Metall. 35 (1987) 439–451.
[19] P.H. Lequeu, P. Gillormini, F. Montheillet, B. Bacroix, J.J. Jonas, Yield surfaces for textured polycrystals – II. Analytical approach, Acta Metall. 35 (5) (1987) 1159–1174.
[20] F. Barlat, O. Cazacu, M. Zyczkowski, D. Banabic, J.W. Yoon, Yield surface plasticity and anisotropy in sheet metals, in: D. Raabe, L.Q. Chen, F. Barlat, F. Roters (Eds.), Continuum Scale Simulation of Engineering Materials, Fundamentals – Microstructures – Process Applications, Wiley, Berlin, 2004, pp. 145–167.
[21] J.W. Yoon, F. Barlat, R.E. Dick, K. Chung, T.J. Kang, Plane stress yield function for aluminum alloy sheets – part II: FE formulation and its implementation, Int. J. Plast. 20 (3) (2004) 495–522.
[22] D. Banabic, F. Barlat, O. Cazacu, T. Kuwabara, Anisotropy and formability, in: Advances in Material Forming, Springer, Paris, 2007, pp. 143–173.
[23] G. Sachs, Zur Ableitung einer Fliessbedingung, Z. Ver. Dent. Ing. 72 (1928) 734–736.
[24] N.L. Svensson, Some observations on the anisotropy of yield strength in cold rolled and annealed metals, Inst. Met. J. 94 (1966) 284–291.
[25] F. Barlat, D.J. Lege, J.C. Brem, A six-component yield function for anisotropic materials, Int. J. Plast. 7 (1991) 693–712.
[26] I.L. Dillamore, W.T. Roberts, Rolling textures in fcc and bcc metals, Acta Metall. 12 (1964) 281–293.
[27] J. Hirsch, Textures and anisotropy in industrial applications of aluminum alloys, Arch. Metall. Mater. 50 (2005) 21–34.
[28] F. Barlat, O. Richmond, Prediction of tricomponent plane stress yield surfaces and associated flow and failure behavior of strongly textured F.C.C. polycrystalline sheets, Mater. Sci. Eng. 95 (1987) 15–29.
[29] U.F. Kocks, G.R. Canova, C.N. Tomé, A.D. Rollett, S.I. Wright, Computer Cod LA-CC-88-6, Los Alamos National Laboratory, 1988.
[30] D.J. Lege, F. Barlat, J.C. Brem, Characterization and modeling of the mechanical behavior and formability of a 2008-T4 sheet sample, Int. J. Mech. Sci. 31 (1989) 549–563.
[31] A.P. Karafillis, M.C. Boyce, A general anisotropic yield criterion using bounds and a transformation weighting tensor, J. Mech. Phys. Solids 41 (1993) 1859–1886.